La Société Savante de l'Aéronautique et de l'Espace

51st 3AF International Conference on Applied Aerodynamics
4 – 6 April 2016. Strasbourg, France

FP32-2016-CHARRIER

SIMULATIONS OF REACTIVE SUPERSONIC/SUBSONIC FLOW INTERACTIONS FOR SPACE LAUNCHER APPLICATIONS ON FLUSEPA SOLVER

Lorris Charrier[(1),(2)], Mathieu Jubera[(1)], Grégoire Pont[(1)], Francesco Grasso[(2)],Simon Marié[(2)], Pierre Brenner[(1)]
[(1)]Airbus Defence & Space
[(2)]DynFluid Laboratory, ENSAM ParisTech

ABSTRACT

In this article, the unstructured, high order finite-volume CFD solver FLUSEPA[1], developed by Airbus Defense & Space, is firstly used to simulate for a steady RANS simulation on a base flow around a four-clustered rockets configuration. Results for several corresponding flight altitudes are compared with NASA experiments and Loci-CHEM simulations in order to estimate FLUSEPA aptitudes to predict time-averaged heat flux and flow structures. Then, unsteady simulations of supersonic H_2/air reacting mixing layer based on the experiment of Miller, Bowman & Mungal are performed with the DDES[2] hybrid RANS[3]/LES[4] model. Three meshes with different cells density are used to study the impact of spatial resolution on the results. Instantaneous and time-averaged concentrations are compared to the combined OH/acetone planar laser-induced fluorescence imaging from experiment.

1. INTRODUCTION

Due to strong complex interactions between plume and atmosphere, space launchers structures are often subject to unsteady loads and heat transfer during ascent phase. For example, at high altitude, the large expansion of plumes (due to low external pressure level) can induce a massive flow separation of the boundary layer of the fuselage. The resulting recirculation bubble can bring up the very hot exhaust gases upwind of the base and threaten the integrity of the structure and equipment. These Plume Induced Flow Separations (PIFS) were observed on several launchers such as Saturn V and are very dependent on the base design. During the development of a new launcher, the prediction of the behavior of this kind of flow structure is primordial. Moreover, its highly unsteady character cannot be predicted efficiently by RANS simulations. Consequently, the use of methods resolving at least the unsteady large energy-containing scales is necessary. In this kind of simulations, the mixing layer between the jet and the atmosphere is particularly challenging. The supersonic hot plume, containing unburnt fuel, mix and reacts with the subsonic and cold oxygen-rich atmosphere. A correct simulation of this type of flow is essential.

In a first part of this paper we give an overview of the FLUSEPA solver, its numerical strategy and models used for turbulence and chemistry. In a second part we present results of RANS and hybrid RANS/LES (HRL) simulations. The RANS simulations deal with a multi-engine configuration with strong flow/plumes interactions. Flow structures and convective heat fluxes on base are compared with NASA computations [8] and experiments [12]. The HRL simulation is relative to a supersonic reacting mixing layer and used as a first approximation for unsteady interaction between plume and atmosphere. In conclusion we discuss about results and probable causes of differences between experiments and simulations. Several approaches are considered and discussed in order to improve these with a minimal additive computational cost.

[1]Registered trademark in France with number 134009261
[2]Delayed Detached Eddy Simulation
[3]Reynolds Averaged Navier-Stokes
[4]Large Eddy Simulation

2. FLUSEPA SOLVER

2.1 General description

FLUSEPA is an high order unstructured finite volume CFD code for the modeling of highly compressible, turbulent, viscous and reactive flows with particles over complex geometries in relative motion. One of the main feature of FLUSEPA is its CHIMERA-like conservative method that avoid the loss conservative variables at grids intersection present in most codes due to interpolation [11, 3, 4, 5]. It allows different parts of the geometry to be meshed independently and then assembled together in a single composite grid by merging the resulting meshes of geometric intersection[5]. In finite volume formulation, for a fixed frame of reference, Navier-Stokes equations can be written as a system of conservation laws for Reynolds-Averaged or filtered variables :

$$\frac{d}{\partial t}\iiint_{\Omega_{CV}} \mathbf{w} d\Omega = -\oiint_{A_{CV}} \mathbf{F}.\mathbf{n} dS + \iiint_{\Omega_{CV}} \mathbf{S} d\Omega \qquad (1)$$

where Ω_{CV} is a fixed control volume with boundary A_{CV}, $\mathbf{n}$ is the outer-oriented unit normal, $\mathbf{w}$ is the conservative variable vector, $\mathbf{F}$ is the flux density tensor and $\mathbf{S}$ is the source terms vector. For a multi-species flow these quantities are given by :

$$\mathbf{w} = (\rho, \rho\mathbf{u}, \rho E, \rho\mathbf{Y}, W_{tm})^{\mathrm{T}} \qquad (2)$$

the flux density tensor can be split into two parts :

$$\mathbf{F} = \mathbf{F_E} + \mathbf{F_D} \qquad (3)$$

where the inviscid flux $\mathbf{F_E}$ is given by :

$$\mathbf{F_E} = (\rho\mathbf{u}, \rho\mathbf{u}\mathbf{u}^{\mathrm{T}} + p\mathbf{I}, \rho\mathbf{u}H, \rho\mathbf{u}\mathbf{Y}^{\mathrm{T}}, F_{tm})^{\mathrm{T}} \qquad (4)$$

and the viscous flux $\mathbf{F_D}$ is

$$\mathbf{F_D} = (0, \tau + \tau_t, (\tau + \tau_t).\mathbf{u} - \mathbf{q} - \mathbf{q_t}, \mathbf{J} + \mathbf{J_t}, 0)^{\mathrm{T}} \qquad (5)$$

In equation (2), W_{tm} is the variables comes from the turbulence model in use. For example, for a $k-\varepsilon$ model, $W_{tm} = \rho k, \rho\varepsilon$. In equation (4), F_{tm} represents the numerical fluxes due to the turbulent variables. In equations (2) and (5), ρ is the density, $\mathbf{u}$ the velocity vector, p the pressure, E the specific total energy, $\mathbf{Y}$ the species mass fractions vector, H the specific total enthalpy, τ the viscous stress tensor, $\mathbf{q}$ the heat flux vector and $\mathbf{J}$ the species molecular diffusive flux tensor. The preceding flow properties have to be integrated as averaged or filtered quantities, according to the equation in use (RANS or LES). More generally, $\mathbf{w}$ represents the resolved part of the flow, i.e, the average field or the large scale of the turbulence flow, for RANS and LES, respectively. In addition, τ_t is the Reynolds/subgrid stress tensor,$\mathbf{q_t}$ the turbulent heat flux and $\mathbf{J_t}$ the species turbulent diffusive flux tensor which model the effect of the "non-resolved" part of the flow on the "resolved" one.

[5]Higher priority level meshes stamping those of lower priority

2.2 Turbulence models

The subgrid stress tensor τ_t in equation 5 is modeled with a Boussinesq eddy viscosity assumption [2]. Numerous models are available in FLUSEPA for the eddy viscosity μ_t. In the following simulation we will use three of them :

- SST $k-\omega$ two equations RANS model [6]
- Spalart-Allmaras one equation RANS model [6]
- Delayed Detached Eddy Simulation (DDES) HRL model

The last model has been recently uppgraded in FLUSEPA and is based on a modified version of Spalart-Allmaras RANS model. In its steady formulation the dissipation term of the modified viscosity $\tilde{\nu}$ transport equation uses the distance from the closest surface d. The HRL version replace this variable by a modified distance $\tilde{d}$ that quickly dissipate $\tilde{\nu}$ (and therefore μ_t) in vortex-dominated regions out of boundary layer [13] The turbulent heat flux $\mathbf{q_t}$ is modeled thanks to a Fourier-like approximation using the turbulent thermal conductivity

$$\lambda_t = \frac{C_p \mu_t}{Pr_t} \qquad (6)$$

where Pr_t is the turbulent Prandtl number chosen to be constant and equal to 0.9. The species turbulent diffusive flux tensor $\mathbf{J_t}$ uses a Fickian-like model with the turbulent diffusion coefficient D_t calculated from constant turbulent Lewis number $Le_t = 1.0$ hypothesis such as

$$D_t = \frac{\lambda_t}{\rho C_p Le_t} \qquad (7)$$

2.3 Chemical kinetic

FLUSEPA uses a finite-rate reversible model for chemical kinetics. *Forward* reaction rate is calculated thanks to Arrhenius equation and *reverse* reaction rate is deduced from equilibrium hypothesis. The thermodynamic properties of gas are temperature-dependent and tabulated. For now, FLUSEPA has no model to represent the effects of unresolved part of the flow on chemistry. It is equivalent to use the averaged or filtered quantities of a control volume in Arrhenius equation without modeling the effects of fluctuations.

2.4 Numerical scheme

Convective fluxes are calculated thanks to the Godunov algorithm that give the exact solution to Riemann problems. A high-order k-exact MUSCL[6] approach is used for reconstruction of variables into cells. In the following

[6]Monotonic Upstream-Centered Scheme for Conservation Laws

simulations a 3rd order spatial upwind scheme, with local 4th order accurate non-dissipative recentering method is used. The blending function between upwind and centered scheme is based on an analytic criterion that ensure stability [13]. Explicit temporal integration is done with a 2nd order Heun scheme along with a local adaptive time stepping algorithm. This method integrate in time each cell with its own characteristic time to minimize the CPU consumption[7]. An advanced Euler scheme, 1st order in precision, is used for implicit temporal integration.

3. RANS NON-REACTIVE SIMULATION FOR HEAT TRANSFER ESTIMATION

The first set of simulations is based on reproduction of wind tunnel tests performed by NASA in 1961 on a multi-engine configuration with hot gases reacting plumes exhaust in supersonic freestream [12]. Results will be also compared to NASA RANS simulations performed with the Loci-CHEM Navier-Stokes CFD solver [8]. These comparisons are aimed at evaluating FLUSEPA capabilities to estimate launcher base thermal environment. Plumes interactions between themselves and with atmosphere can indeed result in high convective heat transfer due to recirculation of hot exhaust gas (Fig.1).

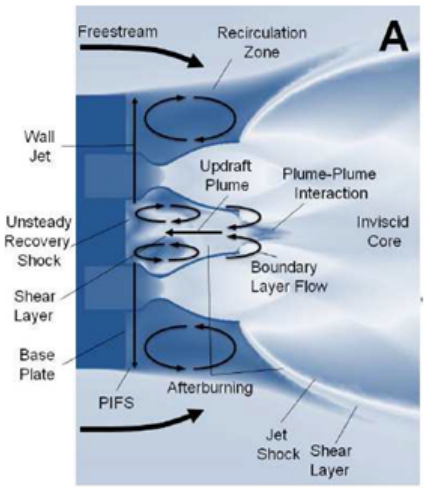

Figure 1: Main flow structures on a 4-clustered rockets configuration (extract from [8])

Two tests conditions corresponding to different flight altitudes have been selected (Tab.1). The base plate from experiment featured radially placed calorimeters giving time-averaged heat flux. Base plate and nozzle dimensions are based on data from experiment (Fig.2) but geometry is extended up to the nose, which is approximated to be roughly equivalent to Loci-CHEM geometry. Sting

[7]It involves several iteration for small cells and few for big ones

Parameters	High altitude	Low altitude
Freestream pressure(Pa)	1676.20	12167.22
Freestream temperature (K)	297.72	
Mach number	2.75	
Simulated altitude (km)	27.65	14.90
Chamber pressure (bar)	41.37	
Chamber temperature (K)	3469.67	

Table 1: Conditions for low and high altitude simulations

present in wind tunnel experiment is not included in the numerical model as it is located significantly up-stream of the base region. Wind tunnel surrounding walls are not modeled and no symmetry planes used.

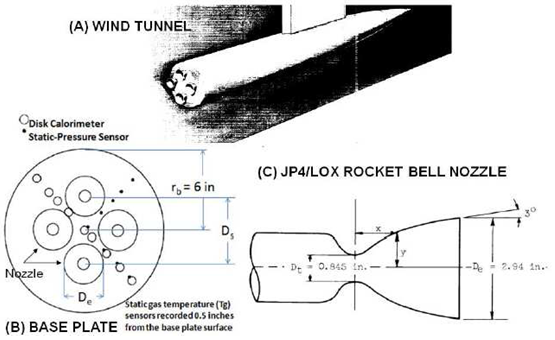

Figure 2: Experimental facility

Our mesh takes advantage of CHIMERA-like overlapping grids approach of FLUSEPA to refine in boundary layer and Interactions zones (Fig.3). The total amount of cells is close to 24.5 million.

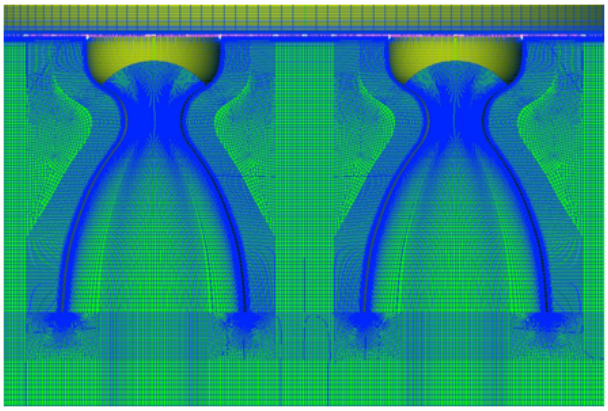

Figure 3: Mesh used near base plate and in nozzle

Both simulations used an isothermal hypothesis for walls. Based on analytic calculations nozzle inner wall temperature was set to 700K. External walls temperature was experimentally determined to be near 340K. NASA Loci-Chem simulations tested several modeling parameters for gas behavior and properties. The following comparison will be based on the ”variable Cp/Cv” case. Our

own study does not take into account chemistry and uses two gaseous species:

- JP-4/LOX replaced by RP-1/LOX (Saturn V gas with closed characteristics)

- Dry air (gamma = 1.4)

Simulations in FLUSEPA were made with a $k-\omega$ SST model and an implicit local time stepping method on 256 cores.

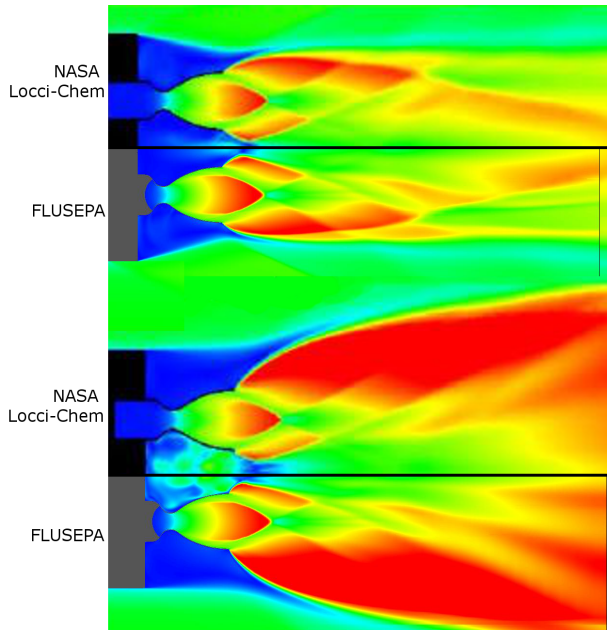

Figure 4: Comparison of Mach number fields between codes at low altitude (top image) and high altitude (bottom image).

FLUSEPA Mach field results close to the plate and downstream are in excellent agreement with Loci-Chem simulations for both low and high altitude (Fig.4). Base heat fluxes are also in good agreement between the two codes (Fig.5).

Mean base heat fluxes compared with experimental measure show an underestimation for both codes at low and high altitude (Fig.6), with significantly better results from FLUSEPA at high altitude. The maximal error is located at base plate center and is near 40% for low altitude and 25% for high altitude case. Simulations with finite-rate chemistry performed by NASA show an improvement in estimation of heat flux (Fig.6), meaning that afterburning seems to play an important role.

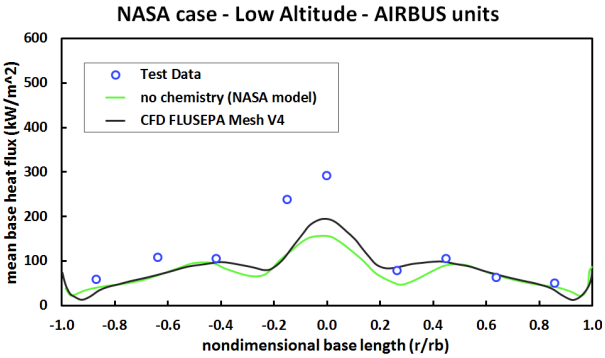

(a) Low altitude

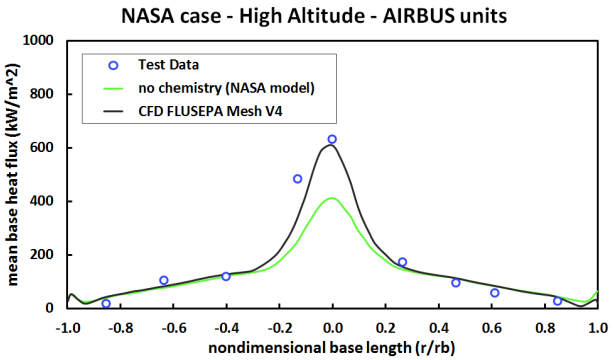

(b) High altitude

Figure 5: Mean base heat flux without chemistry

4. RANS AND DDES SIMULATION OF A COMPRESSIBLE REACTING MIXING LAYER

Unsteady simulations are very important in the design process of a new space launcher as RANS simulations can only give information about averaged flow field. Unsteady loads and heat transfer caused by turbulent fluctuations of pressure, temperature, speed and gas properties can damage or even destroy the structure. Unsteady simulations are more computationally costly than RANS as they require finer meshes and numerous iterations to ensure a good spatial resolution of at least the large scale energy-containing structures over long period of time. Hybrid turbulence models between RANS and LES (or VLES) can be then used to make unsteady simulation computationally affordable with current industrial resources. However, interactions between resolved large scales and unresolved small scales have to be correctly modeled. The strong velocity gradient at the interface between supersonic plume and subsonic/transonic freestream during ascent phase generates a highly compressible, turbulent and reacting mixing layer. When the reattachment point of the recirculating bubble is positioned on the plume the correct simulation of this part of the flow is essential to estimate convective heat transfer

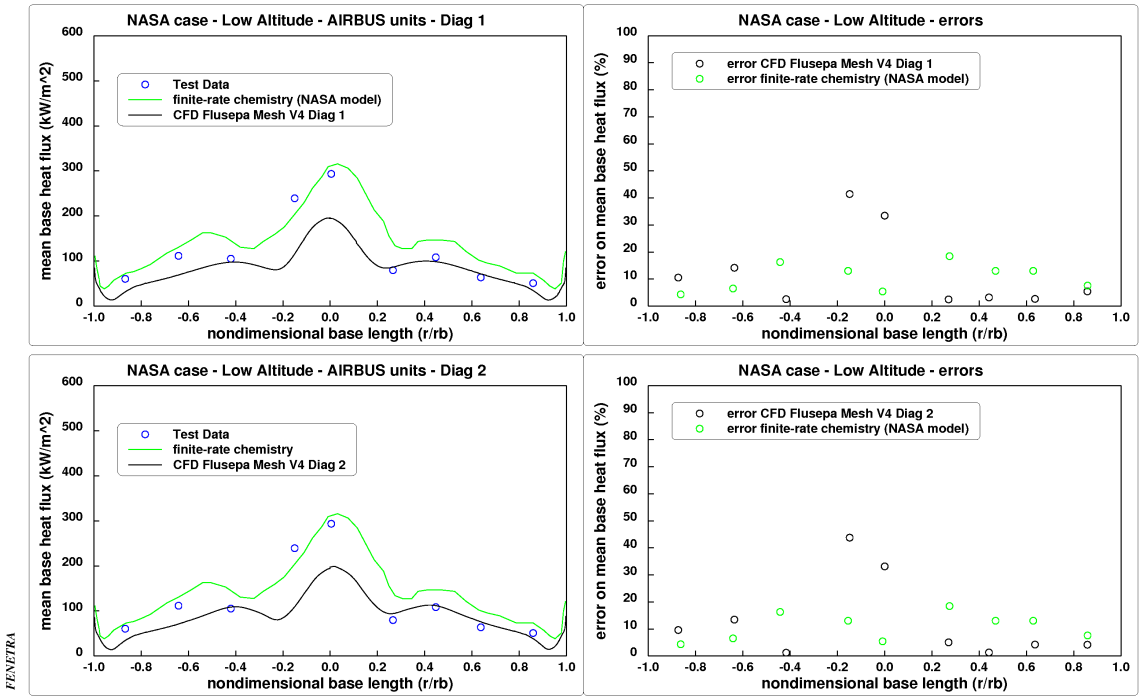

(a) Low altitude

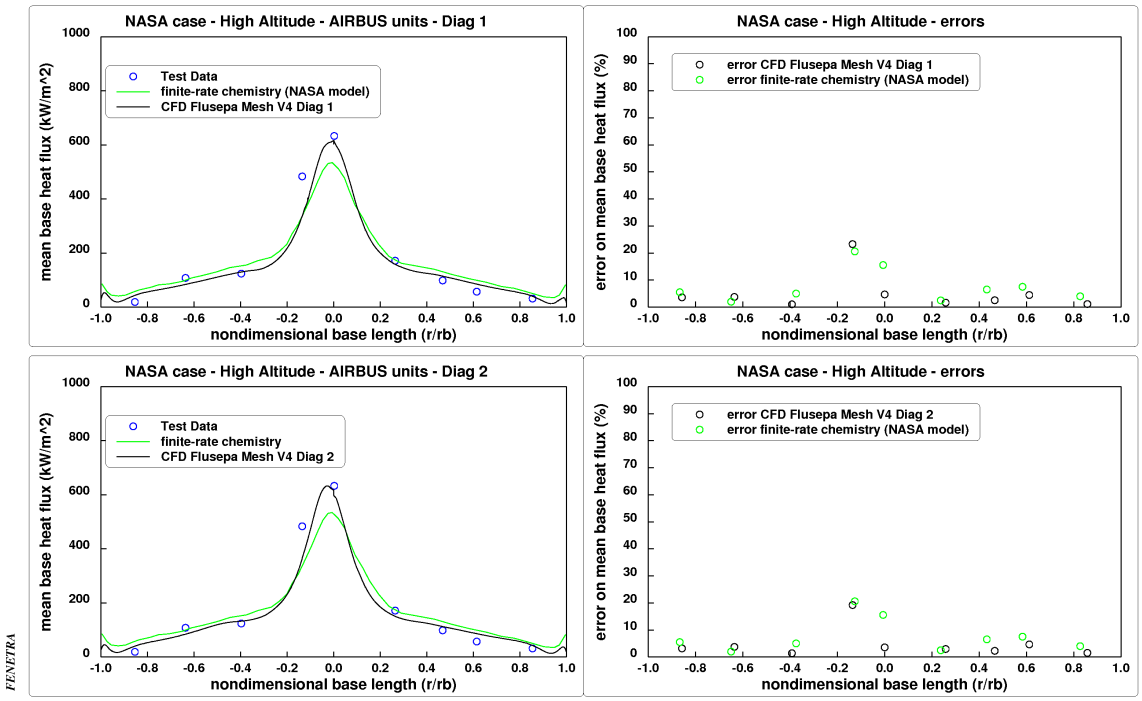

(b) High altitude

Figure 6: Mean base heat flux

in the bubble. In this section, results from Miller experiment [9] on a compressible reacting mixing layer are used as test case for the current DDES turbulence model coupled with simplified mixing and reacting models used in FLUSEPA.

4.1 Simulation details

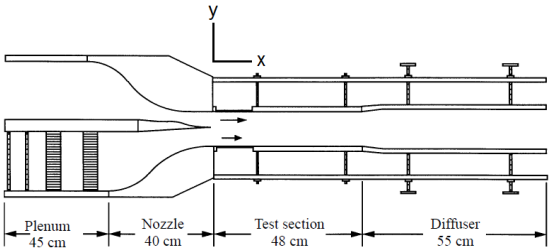

Figure 7: Schematic of the compressible reacting mixing layer facility (extract from [9])

The experiment consists in two co-flowing gas mixtures joining at the end of a splitter tip and mixing in a confined test section (Fig.7). The supersonic hot vitiated air from upper section reacts with a subsonic and cold mixture of nitrogen and hydrogen. The simulation corresponds to the Fast/N_2 case with a convective Mach M_c of 0.7 defined as :

$$M_c = \frac{U1 - U_2}{a_1 + a_2} \tag{8}$$

where U_1 and U_2 denote the velocities of high speed and low speed streams respectively, and a_1 and a_2 the corresponding free-stream sound speed.

	Vitiated air stream	Fuel stream
Total temperature (K)	1790	285
Static temperature (K)	1460	276
Velocity (m/s)	950	150
Mach number	1.23	0.41
Molar composition (%)		
O_2	23	-
H_2O	25	-
N_2	52	90
H_2	-	10
Convective Mach number	0.70	
Static pressure (atm)	0.94	

Table 2: Simulation conditions for the compressible mixing layer

The parameters of each free-stream are listed in table 2. Static pressure probes, Schlieren visualization and combined OH/Acetone PLIF measurement were used to study the mixing layer. Three different meshes were used for DDES calculations with 4, 7 and 13 million cells respectively. In all cases the same mesh was used for RANS

Reaction	A	β	E_a
$O_2+M=O+O+M$	1.2×10^{-05}	-1	117849
$OH+M=H+O+M$	1.4×10^{-05}	-1	100948
$H_2+M=H+H+M$	3.6×10^{-10}	0	95924
$H_2O+M=H+OH+M$	3.6×10^{-08}	0	105059
$H_2O+O=OH+OH$	1.1×10^{-10}	0	18351
$H_2O+H=H2+OH$	1.5×10^{-10}	0	20357
$H+O_2=O+OH$	3.6×10^{-10}	0	16782
$H_2+O_2=OH+OH$	1.7×10^{-11}	0	42778
$H_2+O=H+OH$	6.2×10^{-12}	0	8897

Table 3: Constants used in Arrhenius equation $k_f = AT^{\beta}\exp\left(\frac{-E_a}{R.T}\right)$. The M can represent any specie. We use number of molecules instead of moles as quantity unit.

boundary layer while resolution in HRL free-stream region was increased. Particular attention has been paid to keep an aspect ratio close to unity in VLES mixing region at least for x and y dimensions. An additional coarse mesh with approximately 1 million cells was used for fast implicit RANS calculations. It is based on the 4M mesh with less resolution in z-direction. Splitter tip end thickness has been fixed at 0.8 mm [7] and the small mismatch (80 μm) between upper convergent and test section has been taken into account in geometry. Adiabatic conditions were used for walls as constant temperature would have been hard to define in test section where both hot vitiated air flow and cold fuel interacts with walls. A 6-species, 9-reactions kinetic scheme described in table 3 was used for chemistry, with nitrogen being considered as a passive scalar.

4.2 RANS results

A first RANS calculation is done with 1M and 4M meshes to be used as reference for time-averaged comparison. OH radical concentration can be plot on centerline at 22 cm downstream from splitter tip and compared to experimental data[8] (Fig.8). Results show that RANS gives a good estimation for the curve maximum value and position but underestimates the lower values.

Near-wall OH concentration in simulation is in the same order of magnitude as experiment but presents a higher value. This is probably due to the adiabatic wall that prevents shear heating from being transferred by forced convection and results in temperature increase near wall, leading to a higher concentration of OH. Comparison with pressure probes along top wall give generally satisfying results (Fig.9). Strong variations of pressure are caused by systems of shocks and expansion fans

[8]Experimental curve has been scaled assuming a linear relationship between concentration and LIF emission signal and a maximum concentration of 2000 ppm [9]

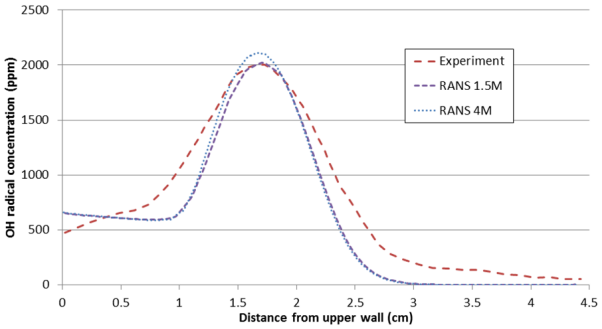

Figure 8: OH concentration comparison on vertical centerline at 22 cm downstream of splitter tip

reflecting between walls and mixing layer. These systems results from supersonic vitiated air flow encountering variation of sections at the entrance of test section because of splitter tip thickness, mixing layer growth and upper wall mismatch. However, the number of experimental probes does not allow us to precisely compare these variations of pressure on wall. Results for 1M and 4M meshes are very similar, which allows us to use the simplest mesh for fast simulations.

On bottom wall, two phenomena may be the cause of the differences between simulation and experiment. First, the lack of information concerning the geometry of bottom section convergent in experiment leads to a bad estimation of the position of the point of minimum pressure, caused by curvature of the wall, which is in our case positioned upstream in the flow. Secondly, the bottom wall was not perfectly parallel to the upper but diverged from horizontal with an angle of 1.6 degree. This information was not present in original paper and was found later in a more complete description of the facility [10]. This is also assumed to be the cause of the augmentation of the pressure present at the end of the supersonic stream, since the test section acts as a divergent. Numerical Schlieren visualization compared to instantaneous Schlieren from experiment shows a good agreement for oblique shock/expansion fan systems (Fig.10). Noise, vignetting effect and acoustic waves in experimental Schlieren make difficult the distinction of structures after few reflections.

4.3 DDES results

The 4M, 7M and 13M meshes were ran simultaneously on 96, 168 and 288 cores respectively. All fields were initialized with a Spalart-Allmaras implicit RANS calculation and then switched to DDES. Each millisecond of simulated physical time needed between 24 and 35h of calculation depending on the mesh. This time scale corresponds approximately to the residence time in test section of a particle at average speed between the two streams. The slowest sub-domain was constrained by CFL condition on the small cells near the mismatch between supersonic upper stream and test section (950 m/s, 80μm). As the effect of this geometrical imperfection is at the origin of oblique shocks system coming from upper wall it cannot be neglected despite its slowing impact on simulation.

Instantaneous snapshots shows two distinctive zones in the mixing layer. First we can see very regular 2D vortices shedding from the splitter tip that are convected over few centimeters. These vortices are then dissipated by the increasing turbulent viscosity used to model the unresolved flow structures before that fully 3D flow structures appear (Fig.11). The vortex shedding is caused by the presence of a shear layer between a recirculation zone trapped at the splitter tip and the supersonic stream. This behavior was also experimentally highlighted by Clemens and Mungal on the same facility (Fig. 12a and 12b). All meshes feature these structures as the resolution has been chosen to be sufficient to resolve vortices the size of splitter tip thickness[9]. Instantaneous numerical Schlieren are in good agreement with experiment[10] (Fig.13). Shocks/expansion fan systems seems to be accurately simulated. Shocks/expansion fan reflections are sensitive to mixing layer structures and their positions and angle vary over time. Mixing layer structures become more detailed with finer meshes but overall mixing layer growth rates seems to be over predicted. This could be caused by a too high value of turbulent viscosity in the shear layer. A new HRL model based on high Reynolds number $k-\varepsilon$ equations is currently being tested in FLUSEPA in order to compare results. The additional information given by a two-equation model could also be useful in later development for better modeling of turbulence/chemistry interactions and turbulent transport.
Unfortunately, low-frequency high-amplitude pressure oscillations in test chamber caused transitions between supersonic and subsonic regime in upper stream, radically modifying mixing layer behavior. These oscillations dampen with time (Fig. 14) and were probably observed in experiment where supersonic regime have been difficult to maintain [10]. As the 4M mesh simulation runs faster than the 7M and 13M, it is the only results where supersonic regime was maintained sufficiently long enough to obtain satisfying time-averaged fields. Numerical Schlieren using gradients of time-averaged density shows shock/expansion fan system similar to RANS results but a different mixing layer growth rate as seen in instantaneous results (Fig.15).

Time-averaged DDES pressures give results similar to RANS for the same mesh resolution (Fig.16). Time-

[9]Thanks to the 4th order local recentering method FLUSEPA can resolve vortices with 6 cells in diameter

[10]A special attention has been payed to reproduce experimental method of visualization by integrating planar xy gradients of refractive index, considered as proportional to density, over the z direction of propagation of colimated light used in experiment

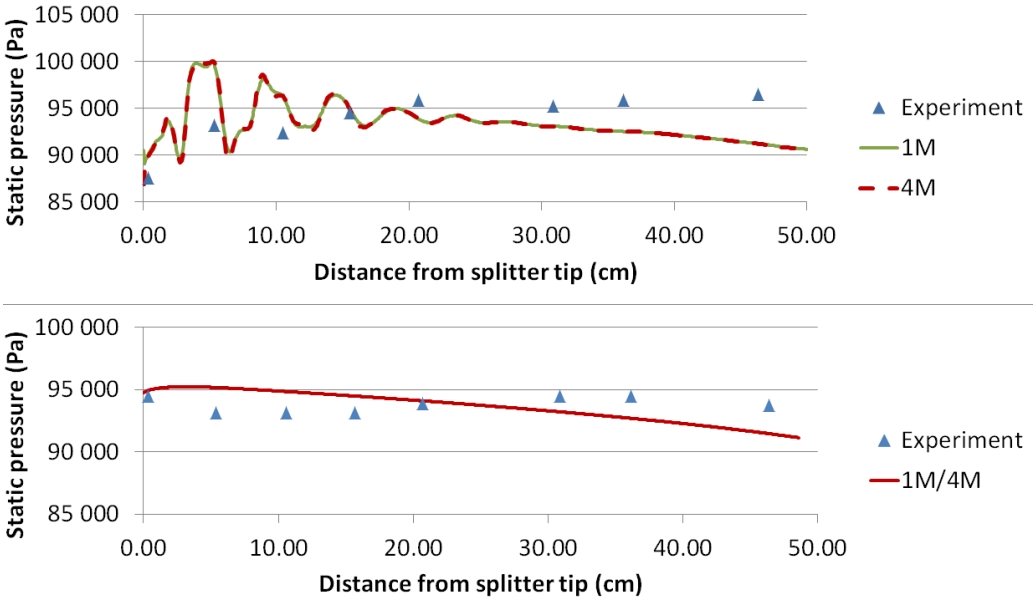

Figure 9: Static pressure on top wall (RANS, 1M and 4M meshes)

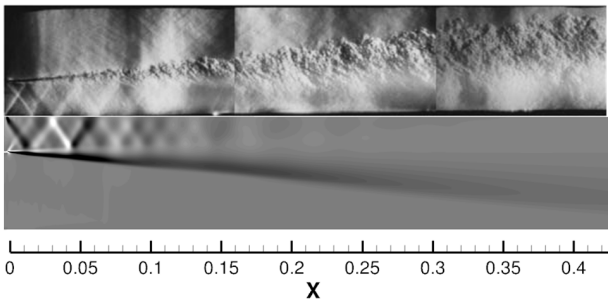

Figure 10: Comparison between experimental (top) and numerical (bottom) Schlieren. Vertical symmetry has been applied to experimental Schlieren to compare shocks/expansion fans positions.

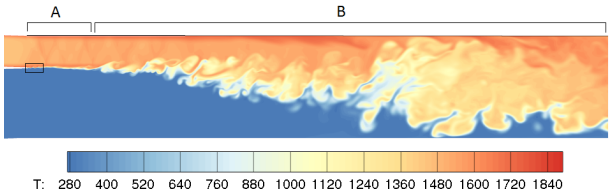

Figure 11: Temperature contour with (A) mostly 2-Dimensional mixing layer structure zone and (B) mixing layer after transition to 3-Dimensional structures. Vortex shedding zone of Fig.12a framed near splitter tip.

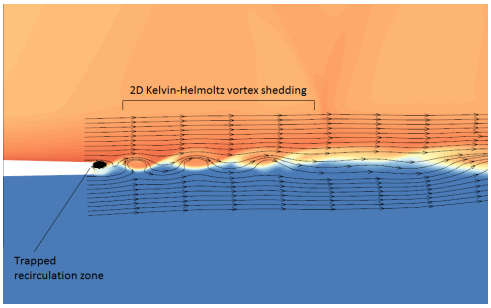

(a) Numerical vortex shedding at convective Mach 0.7 (temperature field)

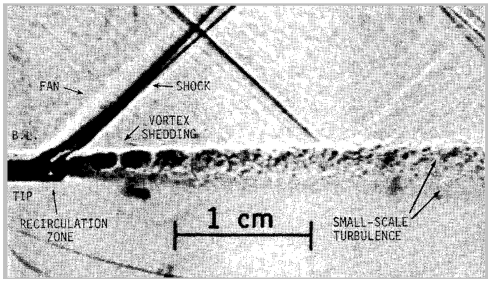

(b) Experimental vortex shedding at convective Mach 0.3 [7]

Figure 12: Observation of numerical and experimental vortex shedding

averaged concentration of OH does not fit well the experimental and RANS results (Fig.17). Several assumptions used for simplification purposes are thought to cause this inaccurate prediction of the species transport and produc-

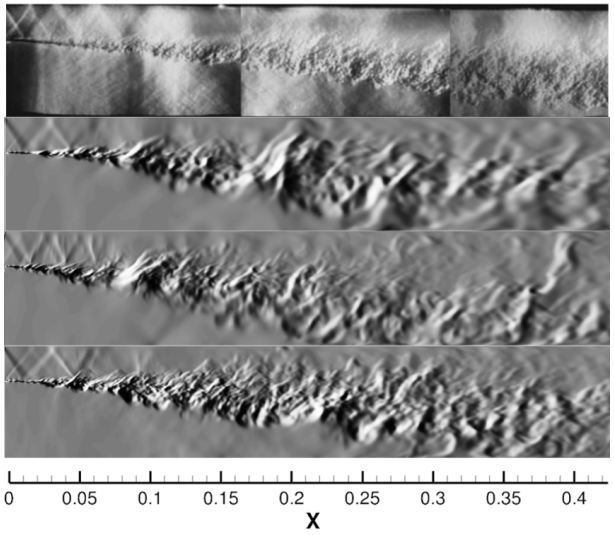

Figure 13: Comparison between experimental (top) and numerical instantaneous Schlieren, from top to bottom 13M, 7M and 4M.

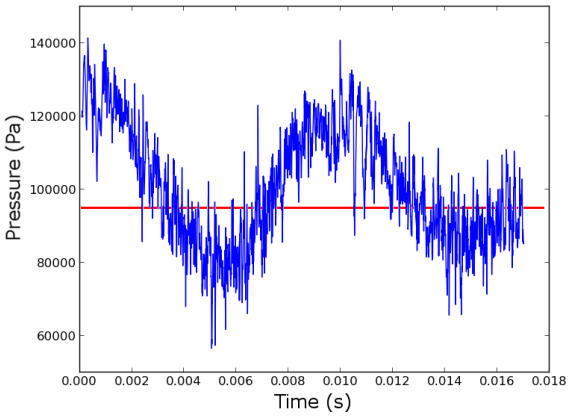

Figure 14: DDES pressure oscillations at the center of the test chamber for 4M mesh. RANS chamber pressure in straight line

tion. First, the mixing layer growth rate seems to be over-predicted. Even if the mesh is fine enough, structures in the flow are too large, resulting in a thickening of the zone where OH radical is present. Secondly, the use of constant turbulent Prandtl and Schmidt number for diffusion by unresolved scales can lead to large inaccuracy in compressible reacting flows [1]. Finally, the lack of sub-grid model may induce a non-negligible error in the reaction rate calculation.

5. CONCLUSION

FLUSEPA solver has been successfully used to estimate time-averaged base heat flux resulting from interaction

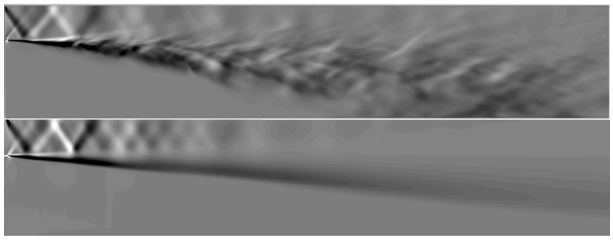

Figure 15: Comparison between RANS numerical Schlieren (top) and calculated from DDES 4M time-averaged density (bottom)

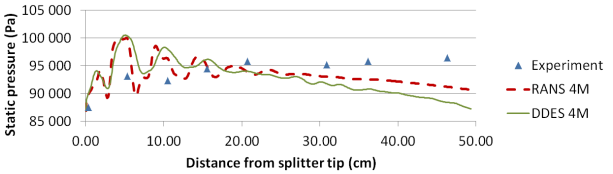

Figure 16: Comparison between RANS top wall pressure and time-averaged pressure from DDES simulation

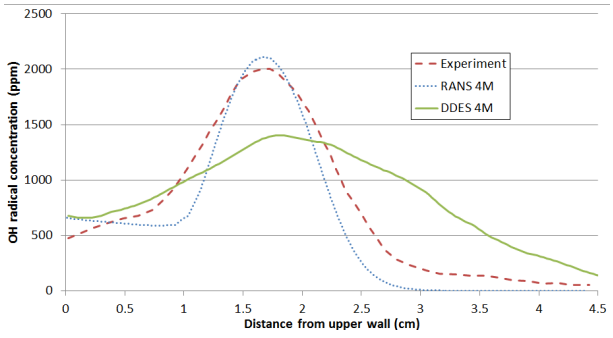

Figure 17: Comparison between RANS numerical Schlieren (top) and calculated from DDES 4M time-averaged density (bottom)

of multiple phenomena on a geometry similar to space launcher. Our results match NASA Loci-CHEM non-reacting estimations but underestimate the experimental heat flux which seems to be very sensitive to afterburning occurring in mixing layer and recirculation zones. In order to asses the FLUSEPA aptitude to simulate such conditions, RANS and DDES calculations have been performed on a compressible reacting mixing layer. Both compressible and turbulent structures are retrieved and time-averaged aerodynamic fields from unsteady simulations matches RANS solution. Moreover, additional information can be extracted thanks to DDES. In particular, 2D vortex shedding from splitter tip and periodic transition between supersonic and subsonic regime were both present in simulation. These transitions disappear after a long simulation time and therefore make unsteady calculations very challenging. Consequently to this day only the simulation on the coarsest mesh has been running a sufficient time in supersonic regime to have usable time-averaged fields. Simulations on 7M and 13M will be soon in fully supersonic regime and effect of mesh convergence on statistical fields will be studied. For now, instantaneous observation on all meshes and time-averaged concentration field on 4M mesh seem to indicate that some assumptions seems to impact the quality of results. Spalart-Allmaras turbulence model in DDES, constant turbulent Prandtl and Schmidt numbers and the lack of sub-grid scale reaction rate term are thought to be in cause. In the next months, a special attention will be payed to improve the transport and reaction models of FLUSEPA for better simulation of compressible unsteady reacting flows.

REFERENCES

[1] R. A. Baurle. Modeling of high-speed reacting flows : established practices and future challenges. *AIAA*, 267, 2004.

[2] J. Boussinesq. Essai sur la théorie des eaux courantes. *Mémoire des savants étrangers, Académie des sciences de Paris*, 1877.

[3] P. Brenner. Three dimensional aerodynamics with moving bodies applied to solid propellant. *27th Joint Propulsion Conference, Sacramento, USA*, 1991.

[4] P. Brenner. Simulation du mouvement relatif de corps soumis a un écoulement instationnaire par une méthode de chavauchement de maillage. In *AGARD conference proceedings 578 : Progress and challenges in CFD methods and Algotithms, Seville, Spain*, 1995.

[5] P. Brenner. A conservative overlapover grid method to simulate tocket stage separation. In *3rd symposium on overset composite grid and solution technology, Los Alamos*, 1996.

[6] S. Catris and B. Aupoix. Density corrections for turbulence models. *Aerospace Science Technologies*, 4:1–11, 2000.

[7] N. Clemens and M. Mungal. Two-and three-dimensional effects in the supersonic mixing layer. *AIAA journal*, 30(4):973–981, 1992.

[8] M. Mehta, F. Canabal, S. B. Tashakkor, and S. D. Smith. Base heating sensitivity study for a 4-cluster rocket motor configuration in supersonic freestream. 2011.

[9] M. Miller, C. Bowman, and M. Mungal. An experimental investigation of the effects of compressibility on a turbulent reacting mixing layer. *Journal of Fluid Mechanics*, 356:25–64, 1998.

[10] M. F. Miller. *An experimental investigation of the effect of compressibility on a turbulent reacting mixing layer*. PhD thesis, Stanford University, 1994.

[11] G. Monge. *Géométrie Descriptive*. PARIS, BAUDOUIN, Imprimeur du Corps lgislatif et de linstitut national, AN VII (1799)., 1799.

[12] N. T. Musial and J. J. Ward. Base flow characteristics for several four-clustered rocket configurations at mach numbers from 2.0 to 3.5. Technical report, DTIC document, 1961.

[13] G. Pont. *Self adaptive turbulence models for unsteady compressible flows*. PhD thesis, Arts et Méters ParisTech, Airbus Defense & Space, 2015.